ADVANCED MATERIALS INTERFACES
Open Access
www.advmatinterfaces.de

Highly Efficient Cash Sterilization with Ultrafast and Flexible Joule-Heating Strategy by Laser Patterning

*Yang Xu, Jing Lin, Yi Chen, Haosong Zhong, Connie Kong Wai Lee, Min Tan, Siyu Chen, Minseong Kim, Elizabeth Wing Yan Poon, Timothy Yee Him Chan, Aidan Qiaoyaxiao Yuan, Miao Tang, Rongliang Yang, Yexin Pan, Ying Fu, and Mitch Guijun Li**

Since ancient times, humans have learned to use fire and other heating methods to fight against dangerous pathogens, like cooking raw food, sterilizing surgical tools, and disinfecting other pathogen transmission media. However, it remains difficult for current heating methods to achieve extremely fast and highly efficient sterilization simultaneously. Herein, an ultrafast and uniform heating-based strategy with outstanding bactericidal performance is proposed. Ultra-precise laser manufacturing is used to fabricate the Joule heater which can be rapidly heated to 90 °C in 5 s with less than 1 °C fluctuation in a large area by real-time temperature feedback control. An over 98% bactericidal efficiency on *S. aureus* for 30 s and on *E. coli* for merely 5 s is shown. The heating strategy shows a 360 times faster acceleration compared to the commonly used steam sterilization from the suggested guidelines by the Centers for Disease Control and Prevention (CDC), indicating that high temperatures with short duration can effectively disinfect microorganisms. As a proof of concept, this heating strategy can be widely applied to sterilizing cash and various objects to help protect the public from bacteria in daily life.

1. Introduction

Humans have been fighting against pandemics caused by bacteria for thousands of years. The bacteria live almost everywhere in the daily environment, among which cash is a perfect place to grow and spread. Due to the close and frequent contact with human skin and the growing human and economic communication between countries, banknotes play a significant role in spreading the bacteria species among communities and continents. Several research works have identified the risk of the bacteria living on banknotes from different countries in the world.[1–4] Therefore, proper and frequent disinfection of banknotes is necessary.

Traditional disinfection methods include chemical, biological, and physical approaches. Alcohol is a widely used chemical to kill many kinds of bacteria on normal occasions. Antibiotics, in another way, act inside living bodies to kill some specific bacteria. However, chemical and biological disinfection suffer from the growing drug resistance of the surviving pathogens. Since the discovery and application of antibiotics, people have been relying increasingly on increasing antibiotic doses and struggling to develop new antibiotics because of the growing drug resistance by generations of artificial selection.[5–7] The abuse of antibiotics and chemicals has given birth to some extremely drug-resistive bacteria like Methicillin-resistant *Staphylococcus aureus* (MRSA), known as super-bacteria.[8–10]

The physical methods, mainly relying on ultraviolet (UV) and heating, prove to be efficient in sterilizing bacteria due to their working scheme. UV radiation tears apart the chemical bonds of DNA or RNA of bacteria and viruses and thus stops them from

Y. Xu, J. Lin, Y. Chen, H. Zhong, C. K. W. Lee, M. Tan, S. Chen, M. Kim, E. W. Y. Poon, T. Y. H. Chan, A. Q. Yuan, M. Tang, R. Yang, Y. Pan, M. G. Li
Research Center on Smart Manufacturing
Division of Integrative Systems and Design
The Hong Kong University of Science and Technology
Clear Water Bay, Kowloon, Hong Kong SAR 999077, China
E-mail: mitchli@ust.hk

The ORCID identification number(s) for the author(s) of this article can be found under https://doi.org/10.1002/admi.202400045

DOI: 10.1002/admi.202400045

Y. Xu, J. Lin, Y. Chen, H. Zhong, C. K. W. Lee, M. Tan, S. Chen, M. Kim, E. W. Y. Poon, T. Y. H. Chan, A. Q. Yuan, M. Tang, R. Yang, Y. Pan, M. G. Li
Hong Kong Branch of Chinese National Engineering Research Center for Tissue Restoration and Reconstruction
The Hong Kong University of Science and Technology
Clear Water Bay, Kowloon, Hong Kong SAR 999077, China

Y. Fu
Department of Pure and Applied Chemistry
University of Strathclyde
Glasgow G1 1XQ, UK

living and reproducing.[11] However, UV cannot penetrate deeply into the inner parts of objects and can only kill the bacteria on the surfaces. Heat will cause irreversible denature of the proteins, which is one of the key substances in bacteria and some viruses and thus deactivate the bacteria, even hiding deep inside, by thermal conduction.[12] However, it is difficult for current disinfection methods to achieve rapid sterilization in a few seconds efficiently without using unrealistic high temperatures or long heating times.[13] Traditional heating-based sterilization, including hot steaming and hot air, requires complicated operations and equipment and consumes much time, which is not suitable for the frequent disinfection of banknotes. Some ultrafast sterilization methods like Pasteurization[14–16] and ultra-high-temperature processing (UHT) cost less time, however, the temperature is not precisely and uniformly controlled in the bulky liquid sample, needless to mention the application range is limited to liquid objects. A more efficient sterilization strategy needs to be developed.

Many researchers have been paying attention to photothermal and Joule heating methods for disinfection, especially since the outbreak of COVID-19. Photothermal heaters convert the energy absorbed from light (usually the sunlight) into heat either by customized nano and microstructures[17–19] or by modulated spectral absorbers that have different absorption and emission characteristics[20,21] among the spectrum to enhance the photothermal effect. Some photothermal absorbers further utilize plasmonic enhancement, radio-frequency heating,[22–24] and nanoparticles to improve the photothermal performance.[25–27] One of the disadvantages of the photothermal heating methods is the limited heating speed. Joule heating, however, makes use of Joule's law of heating that electric current generates heat when passing by a resistor, realizing very fast heating usually in seconds.[28] However, common Joule heating devices can suffer from a problem of the non-uniformly distributed temperature among the heating areas, causing under-heating or over-heating spots, and the lack of flexibility to suit soft and deformable objects including fibers, paper, cloth, etc. Flexible printed circuits (FPC) have become widely used in the electronic industry for flexible applications, however, the traditional fabrication process involves chemicals that generate liquid waste which needs extra pollution processes. Researchers have proposed various novel methods to fabricate flexible circuits while reducing pollution and cost, including metal nano wires[29] and nanoparticle ink printing,[30,31] laser ablation,[32] and laser-seeded deposition.[33–35] We utilize the laser scribing method on the commercially available copper-polyimide film to achieve a cost-efficient and environment-friendly fabrication for rapid and adaptive patterning of flexible devices.

Our research group has been studying laser manufacturing and heat-based sterilization devices for years.[36–39] We have reported photothermal laser-induced graphene surfaces doped with plasmonic enhancement of absorption by nanoparticles for mask sterilization.[40–42] We also reported a laser-induced graphene Joule heater for rapid heating. However, the previous research has not touched on the strategy with a concrete temperature and time profile that can efficiently sterilize the pathogens.

Here, we propose an ultrafast and uniformly-heated Joule-heating sterilization strategy to disinfect banknotes and bacterial-spreading objects. We fabricated the Joule heater from nanosecond laser scribing on commercially available copper-polyimide films. We control the temperature of the heater through real-time feedback and dynamic controlling signals with our self-developed printed circuit board (PCB) modulator. The device can be heated up rapidly to the target temperature of 90 °C in less than 5 s and stabilize within 15 s while keeping at the target temperature for a long duration without drifting. By specially designed conducting patterns, the device can achieve uniform heating with the fluctuation of temperature smaller than 1 °C within the heating area. The bacterial tests show that the prototype device can effectively and efficiently sterilize Escherichia coli *(E. coli)* and Staphylococcus aureus *(S. aureus)* with an ultrafast heating approach while keeping the target sterilized dry and flat, proving its outstanding efficiency and feasibility as a novel disinfection strategy.

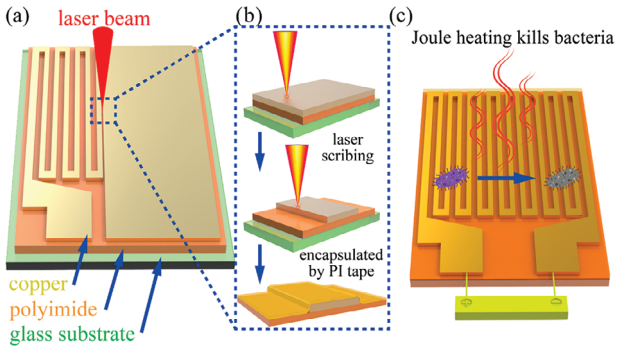

Figure 1. The illustration of the laser ablation fabrication process. a) The laser patterning on the original copper-polyimide film. b) The detailed view of the laser scribing process. c) The illustration of the Joule heating scheme killing bacteria with the fabricated pattern.

2. Results and Discussion

2.1. Fabrication and Characterization

The fabrication process of the laser-patterned copper-polyimide (Cu-PI) heater is shown in **Figure 1**a. The Cu-PI film consists of a 35 μm thick copper layer and a 17 μm thick PI layer cladded tightly. The Cu-PI film is then patterned by a 1064 nm pulsed laser through the laser direct scribing procedures, as elaborated in the experimental section and Note S7 (Supporting Information). After the laser scribing is completed, the exposed copper surface is encapsulated by another layer of PI film for protection, as shown in Figure 1b. The encapsulation layer aims to provide electrical insulation against potential short-circuits and also moist insulation against the oxidization of copper when exposed to a warm and humid environment. The sample can be powered by a power supply for Joule heating to kill bacteria, as shown in Figure 1c. The fabricated sample with a laser-scribed pattern is shown in Figure S1b (Supporting Information).

To study the microstructure of the fabricated Cu-PI pattern, we used optical and electron microscopy for characterization. The optical profile in Figure S1c (Supporting Information) shows the steps in height created by laser scribing. The laser-scribed PI area is ≈30 μm lower than the remaining copper part, which is consistent with the original thickness of the copper layer. As shown in Figure S1d (Supporting Information), the optical microscopic

(OM) image shows the surface detail of the copper pattern and the exposed polyimide after laser ablation. The shining line area is the copper and the dark area with spots is the remaining PI after copper is removed by laser.

The scanning electron microscope (SEM) image shown in Figure S1e (Supporting Information) further illustrates the surface morphology of the laser-scribed polyimide area. The edge of the copper wire is partially ablated as we can tell from the SEM image, and shows pores distributed in the PI area. The overlapped laser spots with a Gaussian distributed beam profile result in the ablation of the copper layer as well as the rough edges of the copper wires, as the overlapping increases the power density delivered to the copper substrate.[43] The overlapping is determined by the laser scanning parameters, including scanning speed, repetition frequency, and the scanning line gap, so that a proper power density is chosen to remove most of the copper layer while causing minimum damage to the bottom PI layer. This laser ablation technique by overlapped laser spots has been reported for metals on tough or thick substrates like glass, quartz, and bulky metals, or thin metal layers, usually with a thickness of a few hundred nanometers.[44–47] It remains a problem, however, for thick metal layers coated on thin substrates like the PI layer to be ablated directly by laser because the high-power laser can easily break the fragile substrate. The SEM image indicates the existence of many micropores on the scribed PI surface created by the high-power laser spots. A nanosecond laser pulse hitting the surface of the copper induces the so-called enhanced plasma absorption effect[48] during which the copper is vaporized and ejected out. The heat absorbed by copper dissipates immediately along with the copper plasma ejection, so the thermal conduction downward to the PI substrate is suppressed.[49,50] The process keeps repeating until the copper layer gets thinner and thinner before the PI substrate is exposed. When the laser spot touches the PI layer, a different mechanism dominates where PI gets overheated due to the relatively slow absorption process that allows heat accumulation. Therefore, the thinner PI layer is extremely fragile under high-power laser pulses. We managed to solve this obstacle by fine-tuning the delivered laser power density. A comparison of the Cu-PI sample under different laser ablation parameters with and without burned defects caused by the high-power laser is shown in Figure S1a (Supporting Information).

To further confirm the removal of the copper layer on the PI substrate, we use energy dispersive X-ray spectroscopy (EDS) to characterize the element distribution of the laser-scribed sample. As shown in Figure S1e (Supporting Information), copper signal accumulates in the central part, which is the copper wire, while little copper exists in the laser-scribed area. Therefore, we can determine that the continuous part of copper wire has an effective width of ≈50 μm and the whole copper wire pattern has a width of ≈170 μm at a designed 200 μm width, considering the rough edges. The UV–vis-NIR transmission spectrum (Figure S2a, Supporting Information) supports the fact that PI absorbs energy from the incident laser beam. The stylus profile (Figure S2b, Supporting Information) also confirms the thickness of the cladded copper layer is ≈30 μm. What is more, the two spikes of the surface height in Figure S2b (Supporting Information) illustrate that there exist higher barriers at the edges of the scribed copper pattern, as reported previously,[32] indicating a copper material accumulation on the scribing line edges due to the laser pulse.

2.2. Heating Performance

2.2.1. Uniform Heating

Joule heating has been a commonly used technique to achieve high-temperature and fast heating with high efficiency due to its energy conversion scheme. Unlike other heating methods, including photothermal or radiative heating,[51–55] Joule heaters directly convert electrical power into heat without loss theoretically. Therefore, Joule heating gained significant attention from researchers who have reported various novel Joule heaters by novel techniques including laser-induced fabrication, metal nanotubes inkjet printing, and coating.[56] A Joule heater based on a laser-induced graphene sheet can achieve a large area of fast heating[57] while another carbon precursor-based Joule heater delivers an extremely high temperature that boosts the chemical breakdown of polymers.[58] Some works can achieve ultrafast heating in a transient state, which takes less than 0.1 s to achieve an extremely high temperature above 2000 K.[59] Similar Joule heaters using silver nanotubes created by inkjet printing obtained ultra-low resistance.[60–63] Joule heaters fabricated with copper nanowires can achieve filtering and Joule heating simultaneously.[64] However, among these Joule heaters, key issues related to heating uniformity and speed still exist. On the one hand, most of the Joule heaters are powered by a constant voltage which limits the freedom of customization of the temperature profile, especially at the beginning of the heating. The difference between the temporary temperature and the final temperature undergoes a nearly exponential decrease, which means that the time consumed has a long tail and temperature drifts before reaching the target temperature. For disinfection cases, the temperature stability and the device durability of the working Joule heater are also necessary. On the other hand, Joule heaters in large areas tend to suffer from spatial non-uniformity more easily. The Joule heating, even on a uniform planar heating device, will lead to non-uniform temperature due to the natural preference for the electrical current to select the conducting path with minimal resistance. Therefore, the surface current density differs from point to point, resulting in a non-uniform temperature profile. We proposed to use a proportional-integral-derivative (PID) controlled heating profile, and an optimized heater pattern to solve the above issues.

To optimize the heating uniformity, we designed a novel geometric pattern of copper wires with electrodes for power supply, as shown in **Figure 2a**. As we mentioned above, a uniform surface cannot guarantee a uniform temperature profile due to unevenly distributed current density. Therefore, we separate the copper conductors forcibly into small segments so that the current has to go through more areas of the heater instead of the smallest path and we can customize the area we want to heat by changing the laser scribing pattern as shown in Figure S3a (Supporting Information). Since each piece of the copper wire plays the role of a tiny heat source while the surrounding PI substrate is the heat conduction and dissipation medium, a temperature gradient builds up between the copper heating element and the surrounding PI, both in-plane (parallel) and out-of-plane (perpendicular). The parallel temperature gradient worsens the uniformity, while the perpendicular temperature gradient improves the uniformity at the bottom side of the PI layer to some degree. Therefore, the heat tends to accumulate in the center of the heater

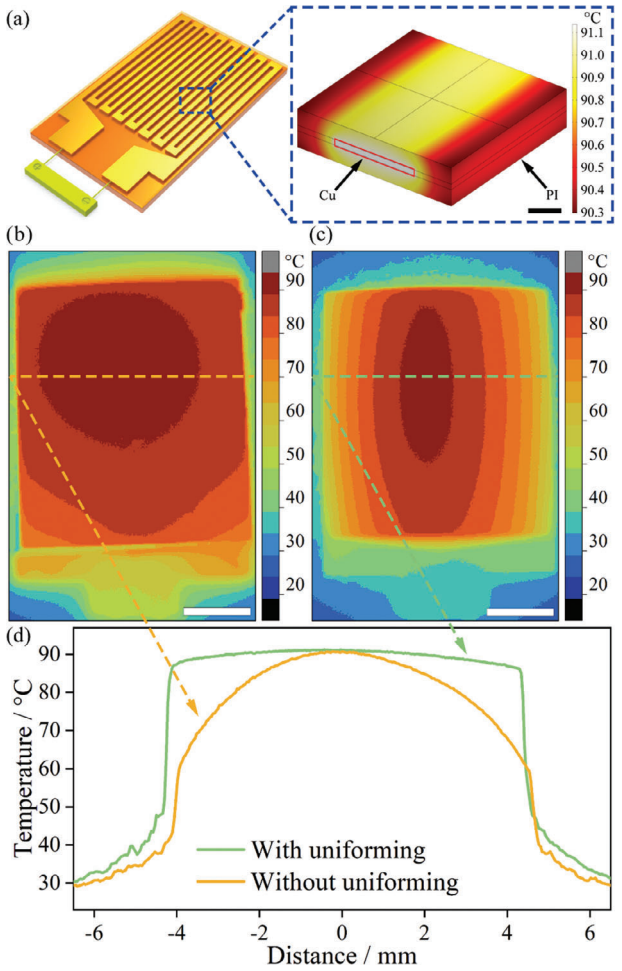

Figure 2. a) The illustration of the heating test of the fabricated sample and the COMSOL simulation of the temperature distribution in the cross-section of one heating wire. IR images showing the temperature distribution on the surface of two samples b) without and c) with the heat uniforming treatment. d) The temperature distribution along one cross-sectional line on the surface of the samples in (b,c). Scale bar (a) is 100 μm. Scale bars (b,c) are 1 cm.

and forms a hot area with a higher temperature, while the surrounding part becomes a cold area. To overcome this challenge, we build a model in COMSOL for simulating the spatial temperature profile along the cross-section of one unit cell of copper-PI structure placed in a periodic model, which is elaborated in Note S8 (Supporting Information), and obtain the optimized copper line width through simulation for an acceptable temperature gradient, as shown in Figure 2a zoomed-in view. The heat generated at the center of a planar heating device dissipates to the environment with more difficulty compared to the edge parts due to the relatively lower temperature differences at the center than at the edges. Therefore, we intentionally increase the width of the copper wires at the center to let the center area generate slightly lower heat than the edges do, to strike a balance between each area in the whole heating device, as discussed in Figure S3b (Supporting Information). We can tell that the sample with the modulated pattern can achieve better spatial uniformity compared to the sample without the modulated pattern, taking the length of the sample of which the temperature falls within the target temperature range of 90 ± 0.5 °C as a quantitative criterion, illustrated by the two arrows in Figure S3b (Supporting Information). Moreover, we can also evaluate the temperature uniformity by the size of the colored area close to the target temperature of 90 °C in Figure 2b,c. In addition, we also added one extra copper tape layer and the PI layer as the heat uniforming layer to better distribute the heat evenly within the surface. The infrared (IR) images shown in Figure 2b,c prove a uniform surface temperature distribution with a difference smaller than 1 °C over an area of 1 cm^2 after applying both heat uniforming techniques. The temperature distribution along the cross-sectional line in both samples also confirms the great improvement in temperature uniformity after adopting our proposed methods, as shown in Figure 2d. Our designed pattern shows a great improvement in temperature uniformity compared to the un-patterned whole-piece metal or LIG heaters, which are not uniform, as shown in Figure S3c–f (Supporting Information). We also used 5 thermocouples to measure the temperature by direct contact mode and the temperature fluctuation is still smaller than 1 °C considering the error caused by the heat conduction due to thermocouple wires, as shown in Figure S4 (Supporting Information).

2.2.2. Ultrafast and Stable Heating

To improve the heating speed and stability, we developed a PID-controlled time profile for heating. With the home-designed PCB and programs, we managed to change the heating power delivered to the heating device with a thermistor to provide the feedback signal. At the very beginning of the heating, we enable a very high power to let the heater temperature increase as soon as possible to reach the target temperature in the shortest possible time. We then cut the heating power when the temperature gets close to the target value to avoid overshoot and protect the heater from damage. Once the temperature reaches the target value, we dynamically fine-tune the delivered power to keep it stabilized within an acceptable range near the target, therefore realizing rapid, precise, and stable heating. As illustrated in **Figure** 3a, we tested the samples in different heating methods with a well-controlled testing setup to compare our heating strategy and device to other heating methods including constant voltage (CV), constant current (CC), air fryer, hot plate, and oven. We found that all other heating methods cannot beat our heater in terms of heating speed. As shown in Figure 3b, our heater with dynamic feedback control shows a rapid increase in the temperature at the beginning of heating, where the temperature jumps up to 90 °C within 5 s and then stabilizes at the target temperature within 15 s. In contrast, all the other heating methods delivered quite slow heating that takes more than 60 s or even longer time to reach the target temperature. As shown in Figure 3c, the heating speed of our heater is one order of magnitude higher than other heating methods, proving its ultrafast heating ability. Moreover, we found that the heating profile shows little temperature drift under 15 min of heating, proving its stability in long operation time, as shown in Figure 3c. The temperature of the constant voltage, constant current, and oven batches keep increasing as long as the power supply is not overloading, thus they cannot

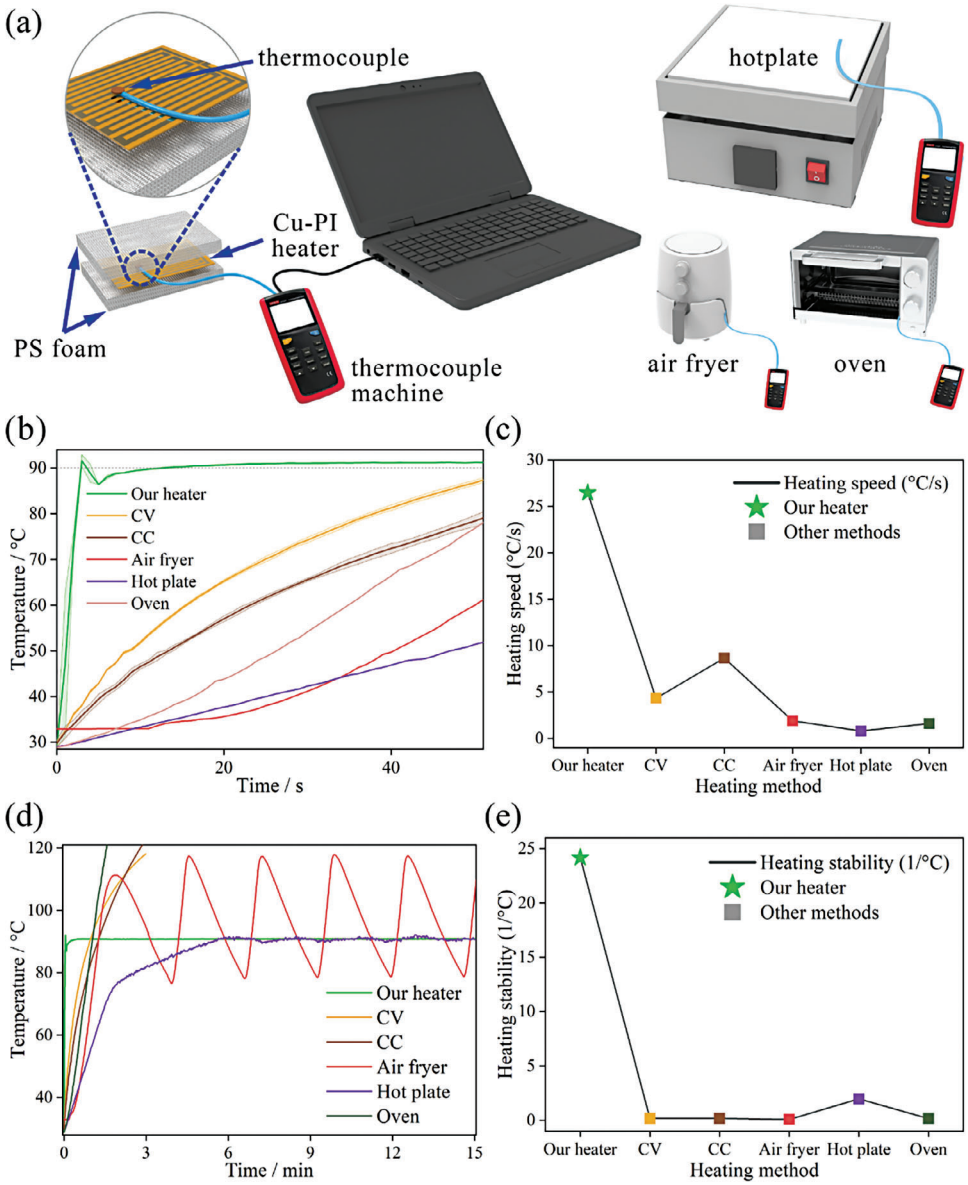

Figure 3. a) The illustration of the heating test using different heating methods with thermocouples for measuring the temperature. b) The temperature profile with time of different heating methods. c) The heating speed extracted from the time profile proves the ultrafast heating speed of our heater. d) The long-time heating profile of different heating methods. e) The heating stability extracted from the long-time profile shows the stability of our heater.

even control the heating near the target temperature, as shown in Figure 3d, while other heating methods like air fryer and hot plate suffer from the huge fluctuations or temperature drifting over time. As shown in Figure 3e, our heater enjoys the highest heating stability compared to other heating methods.

2.2.3. Heating on Multiple Layers

For the disinfection of cash, a common practice is to heat multiple banknotes together to save time. Cash, usually made of cotton paper and polymers,[65] has a loose structure and each banknote contains a lot of wrinkles that can absorb air, which is a thermal insulator, making it difficult for thermal conduction. Yet people place cash in wallets most of the time, and that inspires us to integrate our novel heater into a wallet for convenient disinfection of cash, as illustrated in **Figure** 4a. Some research work showed great heating performance while lacking the testing for thick and layered objects. To confirm the influence of the heating performance of layered objects, we tested the temperature with different layers of filter papers and banknotes. We can tell that thicker filter papers have a slower heating profile compared to thinner filter papers, causing a longer time before reaching the stabilized temperature, as shown in Figure 4b. However, the central temperature decreases linearly with the layer number of filter papers, in a slope of −2.1 °C per layer, as shown in Figure 4c. Therefore, we can determine the temperature at the center of several layers of banknotes (as shown in Figure 4a) and make sure the most

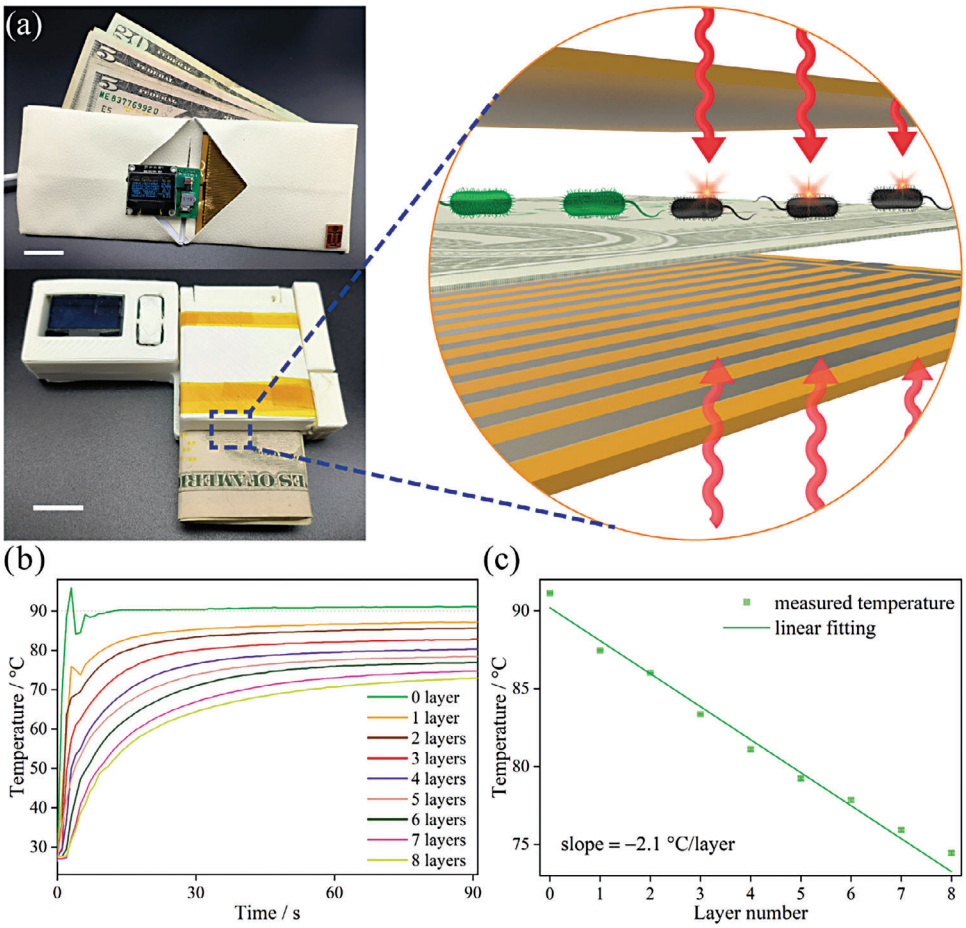

Figure 4. a) The prototype of an ultrafast disinfection wallet with our heater and banknotes inside. The heat generated by double layers of Cu-PI heater penetrates deep through layers of banknotes. b) Temperature profile with heating time for multiple layers of paper. c) Temperature drop for the increasing layer number shows a linear dependence. Scale bars (a) are 2 cm.

centered one still gets sufficient heating, as the temperature drop due to the increasing layers remains within 20 °C for 8 layers of paper. The pressure applied to the objects shows little effect on the final temperature and the heating process, as confirmed in Figure S5 (Supporting Information). We tested the temperature of the paper under different pressures by adding weights and we got almost the same temperature-rising profile. This proves that our PID-controlled Joule heating device is robust to the applied pressure thanks to its self-adaptive feedback ability, so it can maintain high stability in different working environments. During the heating tests, we observed no obvious changes to the banknotes, showing that our heating temperature and time would cause little degradation to the banknotes, compared to the degradation from water and mechanical wear in daily use.[66]

2.3. Flexibility Performance

Our Joule heater consists of several flexible layers in the following order: a bottom layer of PI film as the substrate, a middle layer of copper as the functional Joule heater, and a top layer of PI tape as the encapsulation. Another layer of copper tape is attached to the bottom layer as the heat dissipation layer. To confirm the flexibility of the pristine sample and the sample with PI encapsulation, we conducted the bending test on a motorized positioning with the parameters listed in the experimental section. The Cu-PI samples without encapsulation and with encapsulation present a similar bending angle and performance shown in **Figure 5**a,b, which means that despite the elasticity brought by the PI encapsulation layer, the sample after encapsulation still maintains a similar flexibility compared to the original one. Therefore the PI encapsulation layer does not sacrifice the flexibility much but provides extra protection as noted above. We believe the mechanism for all the interface bonding between each pair of layers is the van der Waals interactions because of the glue between the layers, as shown in Figure 5c,d. The difference in the bondings between each layer should be the bonding strength, as the bottom PI film is bonded with copper by hot lamination with large pressure (premanufactured) while the top PI tape is bonded with copper by hand pressing with limited pressure. To further evaluate the cycle repeatability of the sample, we conducted the bending test on the encapsulated sample 10 000 times with the same motorized positioning system. The SEM cross-section view of interfaces taken from the bending area shown in the yellow frame in Figure 5b

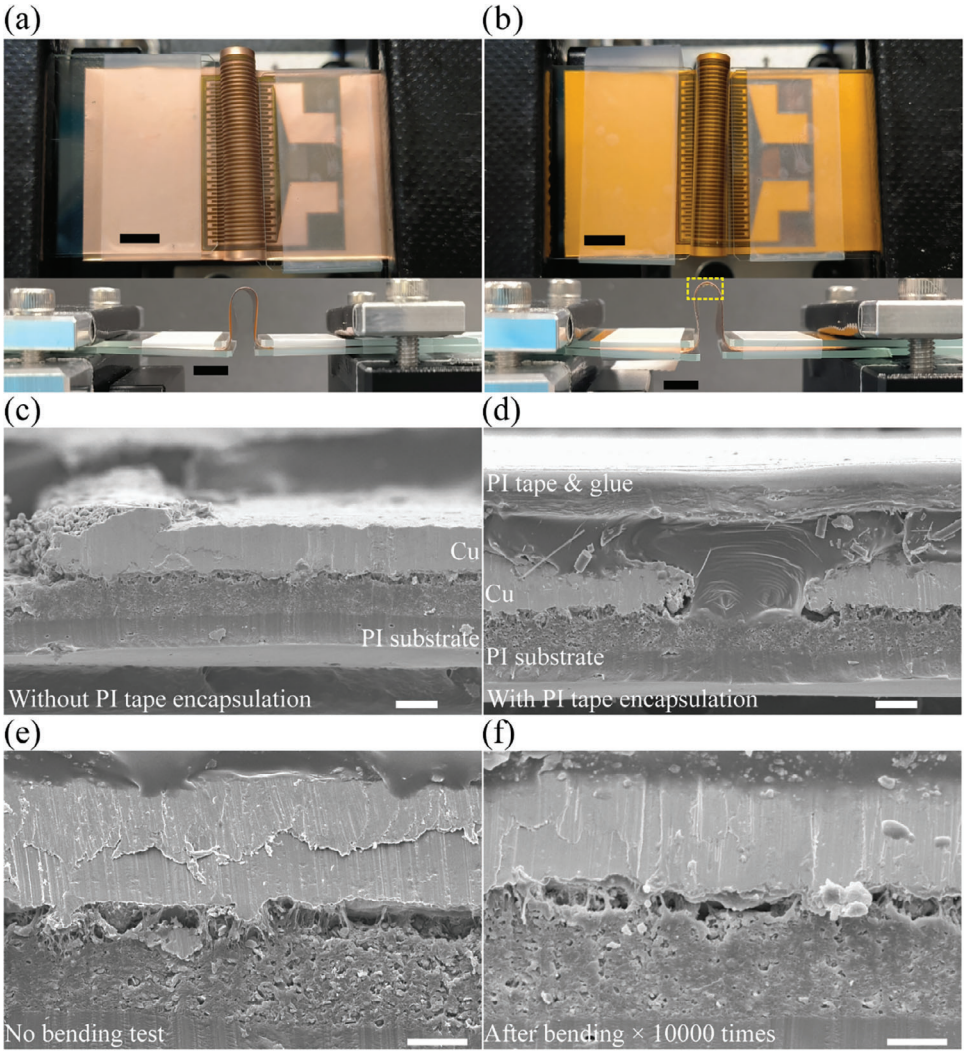

Figure 5. The top and side view of the Cu-PI sample a) without and b) with PI tape encapsulation under bent status. The SEM cross-section view of the Cu-PI sample c) without and d) with PI tape encapsulation. The SEM cross-section view of interfaces of samples with PI tape encapsulation layer e) without and d) with 10 000 times of bending test. Scale bars (a,b) are 5 mm. Scale bars (c,d) are 20 µm. Scale bars (e,f) are 10 µm.

of samples with PI tape encapsulation layer without and with repeated bending confirms that no explicit defects or cracks are introduced to the interfacial layers, as shown in Figure 5e,f.

2.4. Anti-Bacterial Performance

Some works focus on the electrically induced and Joule heating-induced anti-bacterial tests and showed great performances in killing the bacteria on various surfaces including concrete.[67–70] The Joule heating on cash, however, has remained an area that needs investigation. We tested the sterilization performance with the anti-bacterial test, as illustrated in **Figure 6**a. We chose two common pathogenic bacteria: *E. coli* and *S. aureus* as the testing species. We put the filter paper serving as a simulation of banknotes containing the bacteria into our heating device for different heating durations and then washed it out for cultivation. The colony counting results after cultivation in Figure 6b show that under 30 s of heating at 90 °C, the bacteria colony count of *S. aureus* drops by 98%. For *E. coli*, the colony count drops by 99% under 30 s of heating at merely 65 °C while drops by 100% under 5 s of heating at 90 °C as shown in Figure 6c and Figure S6d (Supporting Information), confirming the excellent and ultrafast sterilization performance of our device. It shows a 360 times acceleration compared to the guidelines of using steam-sterilizing for 30 min at 121 °C recommended by the CDC. We also confirmed that *E. coli* can be effectively deactivated when the temperature is higher than 70 °C at a heating duration of only 5 s, which is shown in Figure S6d (Supporting Information), and the colony counting agar plates are shown in Figure S6f (Supporting Information). The integrated device used for bacteria tests and the PCB details are shown in Figure S6a,b (Supporting Information). The bacteria colonies after 18 h of incubation on agar plates are shown in Figure 6d,e for *S. aureus* and *E. coli*, respectively.

However, there still exist some limitations in our study. Although the anti-bacterial tests show good performance, the

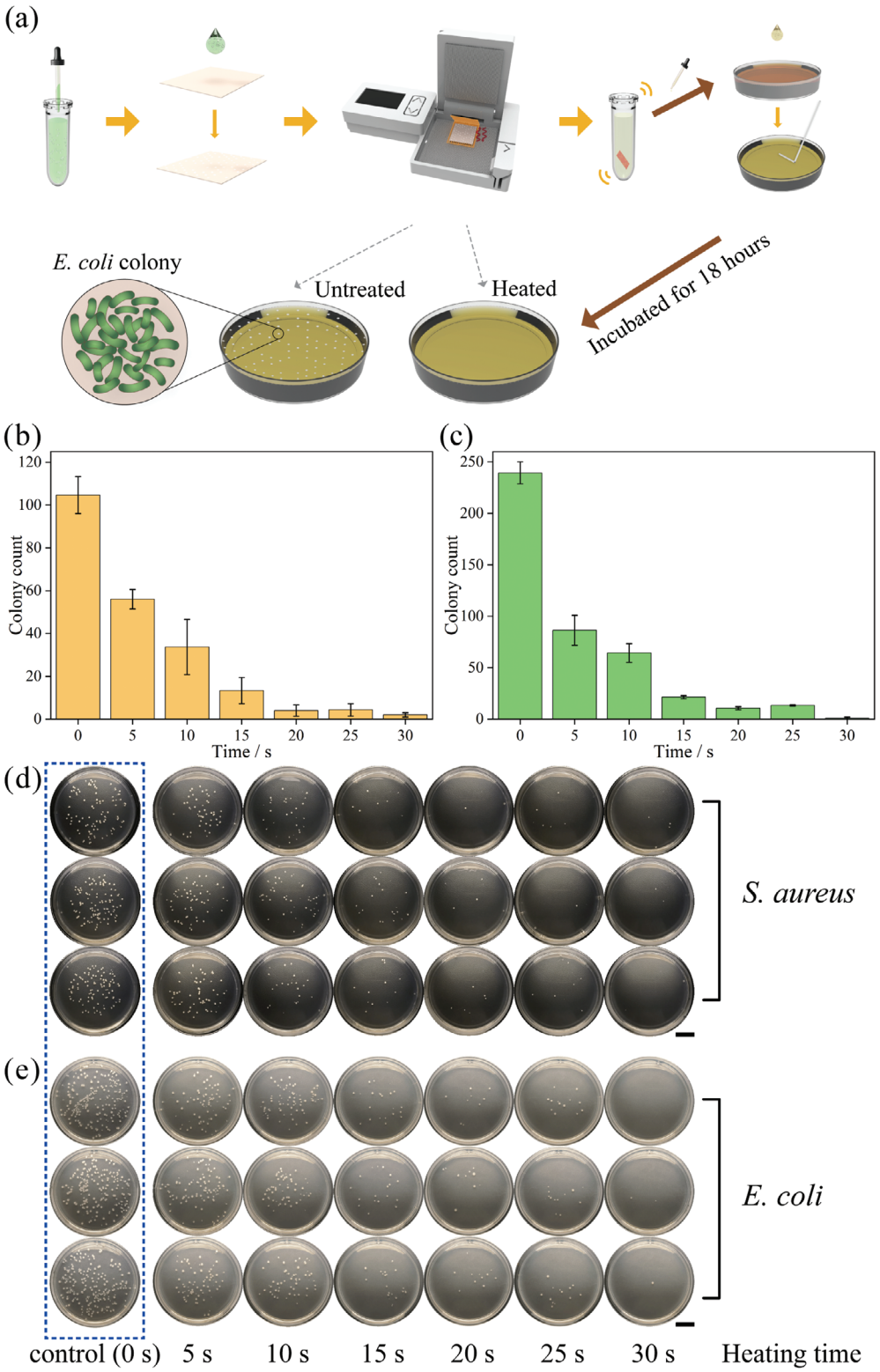

Figure 6. a) The illustration of the bacteria test workflow. Colony count after the sterilization by the device performed on b) *S. aureus* and c) *E. coli*. The optical images of agar plates after incubation for d) *S. aureus* and e) *E. coli* after sterilization by the device. Scale bars in (d,e) are 1 cm.

device still needs to contact the objects to be sterilized as close as possible. It may cause potential doubts for different users sharing the same device for disinfection of some intimate belongings, like thin clothes. In addition, we can design the laser scanning pattern to decrease the copper nanoparticles ejected during the laser scribing process and even make good use of them by back transfer technique.[71] Currently, we use thermal conduction for sterilization, and we plan to improve its heating efficiency by exploiting more channels of thermal exchange, including radiation heating and convection in the future.

3. Conclusion

We designed an ultrafast Joule heater with a uniform temperature profile and efficient sterilization performance against bacteria. We used laser ablation scribing to fabricate the flexible Joule heater. The anti-viral and anti-bacterial tests show ultrafast and highly efficient sterilization performance. Our heater generates no chemical waste during use, causing no environmental burden like chemical sterilizers do. The heat produced by our heater can penetrate deep into the fibers and layers of paper, thus performing better than UV sterilization which can only work for the surfaces. Meanwhile, rapid heating with dynamic control enables a highly efficient and effective sterilization performance. We believe this work will inspire more researchers on Joule heating-related disinfection and shine light on innovative portable devices for sterilization against pathogens by heating.

4. Experimental Section

Materials: The commercially available copper-cladded polyimide (Cu-PI) film consists of 35 µm thick copper and 17 µm thick PI fabricated by hot lamination.

Preparation of Cu-PI Original Sample: A rectangle piece of Cu-PI film was attached to a piece of flat glass and two opposite sides of the film were fixed with scotch tape (810 HK, 3M). It was made sure the target area was closely attached to the glass substrate by tight tape.

Fabrication of Laser Patterned Sample: The laser source was a 1064 nm pulsed laser marking machine. The laser was applied at focal length with the following parameters: scanning speed (300–450 mm s^{-1}), power (12.72 W), filling line gap (2 µm), and repetition frequency (20 kHz). After laser scribing, the Cu-PI film was cleared with absolute ethanol and DI water and then dried by air-blowing and oven. After the laser-scribed Cu-PI sample was cleaned, the copper side was encapsulated with PI tape to prevent short-circuit from accidental electrical contact. Another layer of copper tape was stuck on the back PI layer side as the heat dissipation layer for a more uniform temperature distribution.

Heating Tests: To simulate the disinfection of banknotes, normal paper, filter paper, and surgical masks were selected as the candidates for the heating test. A testing bench was established with two pieces of the same samples as the Joule heating source. The testing objects were cut into squares of 1 cm × 1 cm in size and put in between the two heating elements. The sandwich-like complex was then surrounded by heat insulation layers made of polystyrene (PS) foam and polytetrefluoroethylene PTFE plates to reduce heat loss. An ultra-thin thermocouple (K-type, KAIPUSEN) was used as the temperature sensor to minimize the heat conduction caused by the measurement device. A constant voltage/current and a PID-controlled voltage (from the homemade PCB controller) were applied to the heating elements to obtain the temperature profile at different powering conditions.

Bending Tests: A motorized positioning system (PDV PP110-30-5040 linear motor stage with KZ-100 controller) was used using the following moving profile: accelerate for 1 s at 9 mm s^{-2}, move constantly for 1 s, accelerate for 2 s at −9 mm s^{-2}, move constantly for 1 s, accelerate for 1 s at 9 mm s^{-2}. This profile was the single period of the repeated bending cycle, and the cycle was conducted 10 000 times.

Prototyping: A portable device integrated with a 3D-printed case, homemade PCB controller, and laser-scribed heating elements was built. The electronic details of the PCB are introduced in Figure S6a (Supporting Information). The bacteria tests against *E. coli* and *S. aureus* were conducted.

Bacteria Tests: The filter paper was used as the testing medium and we dropped 10 µL of bacteria suspension with optical density (OD) 1 on the filter paper pieces. After waiting for 5 min in the ambient environment to let the filter paper dry naturally and then it was put into the device for heating of 0–30 s at an interval of 5 s. The processed filter paper was then washed with 1000 µL (for *S. aureus*) and 500 µL (for *E. coli*) of Phosphate-buffered saline (PBS) (0.03 mol L^{-1}, pH 7.2, HKM) for 1 min with a vortex mixer and dilute the eluate at the ratio of 1:500 (for *S. aureus*) and 1:100 (for *E. coli*). A 100 µL of the diluted suspension was dropped onto Petri dishes and cultivated at 37 °C for 18 h for colony counting. The dilution ratio was determined by previous cultivation tests with different dilution ratios for the most suitable one, as shown in Figure S6c (Supporting Information), while the corresponding agar plates are shown in Figure S6e (Supporting Information).

Supporting Information

Supporting Information is available from the Wiley Online Library or from the author.

Acknowledgements

This work was funded by the Hong Kong Research Grants Council under project numbers 25201620 and C6001-22Y, Hong Kong Innovation Technology Commission (ITC) under project number MHP/060/21, Hong Kong Branch of Chinese National Engineering Research Center for Tissue Restoration and Reconstruction (ITC-CNERC14SC01), Materials Characterization and Preparation Facility, and State Key Laboratory of Advanced Displays and Optoelectronics Technologies, The Hong Kong University of Science and Technology. Y. Fu thanks for the funding by Royal Society (RGS/R2/222050) and Royal Society of Chemistry (E22-4714717313).

Conflict of Interest

The authors declare no conflict of interest.

Author Contributions

M.L. conceived and designed the research. Y.X. discussed with M.L. on details and facilitated the experiments and characterizations. J.L. helped with the preparation of the Cu-PI sample. H.Z. helped with the PCB design and programming. K.L. and M.K. helped with the illustration. Y.C., M.T., and S.C. helped with the characterization of SEM. T.C. helped with the characterization of the microscope. E.P. helped with the bacteria tests. A.Y., M.T., and Y.P. helped with the experimental data acquisition. R.Y. and Y.F. helped with the draft preparation.

Data Availability Statement

The data that support the findings of this study are available from the corresponding author upon reasonable request.

Keywords

anti-bacteria, cash disinfection, Joule heating, laser patterning

Received: January 16, 2024
Revised: March 20, 2024
Published online:

[1] L. Vayachuta, R. Thiramanas, P. Prompinit, S. Du-a-man, D. Viboonratanasri, C. Chotsuwan, *ACS Appl Polym Mater* **2021**, *3*, 5105.
[2] J. Lin, W. Jiang, Y. Shi, W. Cai, *ACS Omega* **2021**, *6*, 3499.
[3] H. Gedik, T. A. Voss, A. Voss, *Antimicrob Resist Infect Control* **2013**, *2*, 22.
[4] Y. Heshiki, T. Dissanayake, T. Zheng, K. Kang, Y. Ni, Z. Xu, C. Sarkar, P. C. Y. Woo, B. K. C. Chow, D. Baker, A. Yan, C. J. Webster, G. Panagiotou, J. Li, *Front Microbiol* **2017**, *8*, 632.
[5] H. C. Neu, *Science* **1992**, *257*, 1064.
[6] S. B. Levy, B. Marshall, *Nat. Med.* **2004**, *10*, S122.
[7] L. L. Ling, T. Schneider, A. J. Peoples, A. L. Spoering, I. Engels, B. P. Conlon, A. Mueller, T. F. Schäberle, D. E. Hughes, S. Epstein, M. Jones, L. Lazarides, V. A. Steadman, D. R. Cohen, C. R. Felix, K. A. Fetterman, W. P. Millett, A. G. Nitti, A. M. Zullo, C. Chen, K. Lewis, *Nature* **2015**, *517*, 455..
[8] S. R. Harris, E. J. Feil, M. T. G. Holden, M. A. Quail, E. K. Nickerson, N. Chantratita, S. Gardete, A. Tavares, N. Day, J. A. Lindsay, J. D. Edgeworth, H. de Lencastre, J. Parkhill, S. J. Peacock, S. D. Bentley, *Science* **2010**, *327*, 469.
[9] A. S. Lee, H. de Lencastre, J. Garau, J. Kluytmans, S. Malhotra-Kumar, A. Peschel, S. Harbarth, *Nat. Rev. Dis. Primers* **2018**, *4*, 1.
[10] H. F. Chambers, F. R. DeLeo, *Nat. Rev. Microbiol.* **2009**, *7*, 629.
[11] M. Wegener, M. J. Hansen, A. J. M. Driessen, W. Szymanski, B. L. Feringa, *J. Am. Chem. Soc.* **2017**, *139*, 17979.
[12] S. Riddell, S. Goldie, A. Hill, D. Eagles, T. W. Drew, *Virol J* **2020**, *17*, 145.
[13] M. F. Espinosa, A. N. Sancho, L. M. Mendoza, C. R. Mota, M. E. Verbyla, *International Journal of Hygiene and Environmental Health* **2020**, *230*, 113595.
[14] K. Krishnamurthy, H. K. Khurana, J. Soojin, J. Irudayaraj, A. Demirci, *Compr Rev Food Sci Food Saf* **2008**, *7*, 2.
[15] F. F. Anhê, A. Marette, *Nat. Med.* **2017**, *23*, 11.
[16] I. Jeon, E. C. Ryberg, P. J. J. Alvarez, J.-H. Kim, *Nat. Sustain.* **2022**, *5*, 801.
[17] M. Shi, Z. Song, J. Ni, X. Du, Y. Cao, Y. Yang, W. Wang, J. Wang, *ACS Nano* **2023**, *17*, 2029.
[18] Y. Jung, S. Jeong, J. Ahn, J. Lee, S. H. Ko, *Small* **2023**, *20*, 2304338.
[19] J. F. Torres, K. Tsuda, Y. Murakami, Y. Guo, S. Hosseini, C.-A. Asselineau, M. Taheri, K. Drewes, A. Tricoli, W. Lipiński, J. Coventry, *Energy Environ. Sci.* **2022**, *15*, 1893.
[20] P.-C. Hsu, C. Liu, A. Y. Song, Z. Zhang, Y. Peng, J. Xie, K. Liu, C.-L. Wu, P. B. Catrysse, L. Cai, S. Zhai, A. Majumdar, S. Fan, Y. Cui, *Sci. Adv.* **2017**, *3*, e1700895.
[21] H. Luo, Y. Zhu, Z. Xu, Y. Hong, P. Ghosh, S. Kaur, M. Wu, C. Yang, M. Qiu, Q. Li, *Nano Lett.* **2021**, *21*, 3879.
[22] C. B. Sweeney, A. G. Moran, J. T. Gruener, A. M. Strasser, M. J. Pospisil, M. A. Saed, M. J. Green, *ACS Appl. Mater. Interfaces* **2018**, *10*, 27252.
[23] J. C. Gerringer, A. G. Moran, T. Habib, M. J. Pospisil, J. H. Oh, B. R. Teipel, M. J. Green, *ACS Appl. Nano Mater.* **2019**, *2*, 7032.
[24] L. Jauffred, A. Samadi, H. Klingberg, P. M. Bendix, L. B. Oddershede, *Chem. Rev.* **2019**, *119*, 8087.
[25] J. Zhou, Y. Jiang, S. Hou, P. K. Upputuri, D. Wu, J. Li, P. Wang, X. Zhen, M. Pramanik, K. Pu, H. Duan, *ACS Nano* **2018**, *12*, 2643.
[26] L. Zhou, Y. Tan, D. Ji, B. Zhu, P. Zhang, J. Xu, Q. Gan, Z. Yu, J. Zhu, *Sci. Adv.* **2016**, *2*, e1501227.
[27] S. Chen, Z. Sun, W. Xiang, C. Shen, Z. Wang, X. Jia, J. Sun, C.-J. Liu, *Nano Energy* **2020**, *76*, 104998.
[28] W. Tang, Z. Chen, Z. Song, C. Wang, Z. a. Wan, C. L. J. Chan, Z. Chen, W. Ye, Z. Fan, *ACS Nano* **2022**, *16*, 10968.
[29] S. Hong, H. Lee, J. Lee, J. Kwon, S. Han, Y. D. Suh, H. Cho, J. Shin, J. Yeo, S. H. Ko, *Adv. Mater.* **2015**, *27*, 4744.
[30] V.-T. Tran, Y. Wei, H. Yang, Z. Zhan, H. Du, *Nanotechnology* **2017**, *28*, 095204.
[31] J. Du, B. Zhang, M. Jiang, Q. Zhang, K. Zhang, Y. Liu, L. Wang, W. Jiang, *Adv. Funct. Mater.* **2023**, *33*, 2213564.
[32] D. Paeng, J.-H. Yoo, J. Yeo, D. Lee, E. Kim, S. H. Ko, C. P. Grigoropoulos, *Adv. Mater.* **2015**, *27*, 2762.
[33] J. Kwon, H. Cho, Y. D. Suh, J. Lee, H. Lee, J. Jung, D. Kim, D. Lee, S. Hong, S. H. Ko, *Adv. Mater. Technol.* **2017**, *2*, 1600222.
[34] J. Ren, D. Li, Y. Zhang, W. Yang, H. Nie, Y. Liu, *ACS Appl. Electron. Mater.* **2022**, *4*, 2191.
[35] H. Pan, D. J. Hwang, S. H. Ko, T. A. Clem, J. M. J. Fréchet, D. Bäuerle, C. P. Grigoropoulos, *Small* **2010**, *6*, 1812.
[36] G. Li, X. Mo, W.-C. Law, K. C. Chan, *J. Mater. Chem. A* **2019**, *7*, 4055.
[37] G. Li, *J. Appl. Phys.* **2020**, *127*, 010901.
[38] D. Xu, H. Zhong, M. G. Li, S. S. To, L. Lu, *Carbon* **2023**, *204*, 231.
[39] G. Li, W.-C. Law, K. C. Chan, *Green Chem.* **2018**, *20*, 3689.
[40] N. Jiang, Y. Wang, K. C. Chan, C. Y. Chan, H. Sun, G. Li, *Glob Chall* **2020**, *4*, 1900054.
[41] H. Zhong, Z. Zhu, P. You, J. Lin, C. F. Cheung, V. L. Lu, F. Yan, C.-Y. Chan, G. Li, *ACS Nano* **2020**, *14*, 8846.
[42] H. Zhong, Z. Zhu, J. Lin, C. F. Cheung, V. L. Lu, F. Yan, C.-Y. Chan, G. Li, *ACS Nano* **2020**, *14*, 6213.
[43] Y. Chyan, R. Ye, Y. Li, S. P. Singh, C. J. Arnusch, J. M. Tour, *ACS Nano* **2018**, *12*, 2176.
[44] Z. Li, O. Allegre, L. Li, *Light Sci Appl* **2022**, *11*, 339.
[45] Y. Hanada, K. Sugioka, H. Takase, H. Takai, I. Miyamoto, K. Midorikawa, *Appl. Phys. A* **2005**, *80*, 111.
[46] Q. Yang, Z. Hu, M.-H. Seo, Y. Xu, Y. Yan, Y.-H. Hsu, J. Berkovich, K. Lee, T.-L. Liu, S. McDonald, H. Nie, H. Oh, M. Wu, J.-T. Kim, S. A. Miller, Y. Jia, S. Butun, W. Bai, H. Guo, J. Choi, A. Banks, W. Z. Ray, Y. Kozorovitskiy, M. L. Becker, M. A. Pet, M. R. MacEwan, J.-K. Chang, H. Wang, Y. Huang, J. A. Rogers, *Nat. Commun.* **2022**, *13*, 6518.
[47] C. Gao, L. Zhang, Y. Hou, Y. Zheng, *Adv. Mater.* **2023**, *35*, 2304080.
[48] Y. Hanada, K. Sugioka, K. Obata, S. V. Garnov, I. Miyamoto, K. Midorikawa, *J. Appl. Phys.* **2006**, *99*, 043301.
[49] C. S. Montross, T. Wei, L. Ye, G. Clark, Y.-W. Mai, *Int J Fatigue* **2002**, *24*, 1021.
[50] Q.-L. Xiong, T. Kitamura, Z. Li, *J. Appl. Phys.* **2019**, *125*, 194302.
[51] P. Tao, G. Ni, C. Song, W. Shang, J. Wu, J. Zhu, G. Chen, T. Deng, *Nat. Energy* **2018**, *3*, 1031.
[52] G. Ni, G. Li, S. V. Boriskina, H. Li, W. Yang, T. Zhang, G. Chen, *Nat. Energy* **2016**, *1*, 16126.
[53] Y. Peng, W. Zhao, F. Ni, W. Yu, X. Liu, *ACS Nano* **2021**, *15*, 19490.
[54] Z. Yu, S. Cheng, C. Li, L. Li, J. Yang, *ACS Appl. Mater. Interfaces* **2019**, *11*, 32038.
[55] Z. Wang, H. Yang, Y. Li, X. Zheng, *ACS Appl. Mater. Interfaces* **2020**, *12*, 15726.
[56] L. Wu, L. Wang, Z. Guo, J. Luo, H. Xue, J. Gao, *ACS Appl. Mater. Interfaces* **2019**, *11*, 34338.
[57] L. Huang, M. Gu, Z. Wang, T. W. Tang, Z. Zhu, Y. Yuan, D. Wang, C. Shen, B. Z. Tang, R. Ye, *Adv. Funct. Mater.* **2021**, *31*, 2101195.
[58] Q. Dong, A. D. Lele, X. Zhao, S. Li, S. Cheng, Y. Wang, M. Cui, M. Guo, A. H. Brozena, Y. Lin, T. Li, L. Xu, A. Qi, I. G. Kevrekidis, J. Mei, X. Pan, D. Liu, Y. Ju, L. Hu, *Nature* **2023**, *616*, 488.
[59] Q. Dong, Y. Yao, S. Cheng, K. Alexopoulos, J. Gao, S. Srinivas, Y. Wang, Y. Pei, C. Zheng, A. H. Brozena, H. Zhao, X. Wang, H. E. Toraman, B. Yang, I. G. Kevrekidis, Y. Ju, D. G. Vlachos, D. Liu, L. Hu, *Nature* **2022**, *605*, 470.
[60] M. Zhu, X. Yan, X. Li, L. Dai, J. Guo, Y. Lei, Y. Xu, H. Xu, *ACS Appl. Mater. Interfaces* **2022**, *14*, 45697.

[61] P.-H. Wang, S.-P. Chen, C.-H. Su, Y.-C. Liao, *RSC Adv.* **2015**, *5*, 98412.
[62] M. Li, S. Sinha, S. Hannani, S. B. Walker, M. LeMieux, P. W. Leu, *ACS Appl. Electron. Mater.* **2023**, *5*, 173.
[63] T.-B. Song, Y. Chen, C.-H. Chung, Y. Yang, B. Bob, H.-S. Duan, G. Li, K.-N. Tu, Y. Huang, Y. Yang, *ACS Nano* **2014**, *8*, 2804.
[64] S. Han, J. Kim, Y. Lee, J. Bang, C. G. Kim, J. Choi, J. Min, I. Ha, Y. Yoon, C.-H. Yun, M. Cruz, B. J. Wiley, S. H. Ko, *Nano Lett.* **2022**, *22*, 524.
[65] H. Wang, L. Sun, *Acc Mater Res* **2021**, *2*, 1.
[66] B. J. Jones, J. W. Cammidge, C. Evans, G. Scott, P. B. Sherriffs, F. Breen, P. M. B. Andersen, K. T. Popov, J. O'Hara, *Science & Justice* **2022**, *62*, 644.
[67] C. D. Powell, L. Pisharody, C. Thamaraiselvan, A. Gupta, H. Park, B. A. Tesfahunegn, C. P. Sharma, M. N. Kleinberg, R. Burch, C. J. Arnusch, *ACS Appl. Nano Mater.* **2022**, *5*, 11923.
[68] C. P. Sharma, C. J. Arnusch, *Carbon* **2022**, *196*, 102.
[69] S. P. Singh, Y. Li, A. Be'er, Y. Oren, J. M. Tour, C. J. Arnusch, *ACS Appl. Mater. Interfaces* **2017**, *9*, 18238.
[70] A. Gupta, C. P. Sharma, C. Thamaraiselvan, L. Pisharody, C. D. Powell, C. J. Arnusch, *ACS Appl. Mater. Interfaces* **2021**, *13*, 59373.
[71] C. Zhang, Y. Yu, Y. Cao, X. Wei, S. Su, W. Liu, *Opt. Laser Technol.* **2021**, *138*, 106849.